JOURNAL OF GEOPHYSICAL RESEARCH, VOL. 88, NO. C10, PAGES 6053–6065, JULY 20, 1983

The Response of Antarctic Icebergs to Ocean Waves

PETER WADHAMS AND MONICA KRISTENSEN

Scott Polar Research Institute, University of Cambridge
Cambridge CB2 1ER, England

OLAV ORHEIM

Norsk Polarinstitutt, 1330 Oslo Lufthavn, Norway

The heave, tilt, and strain responses of three Antarctic tabular icebergs to ocean waves were measured during a 1980–1981 cruise of HMS *Endurance* to the South Atlantic. The three icebergs, located near the South Sandwich and South Orkney islands, were instrumented with accelerometers, tiltmeters, and wire strainmeters, while a Waverider buoy was used to record the ocean wave field. The thickness of the icebergs was surveyed by a helicopter-borne radio echo sounder. The heave response occurred mainly at the swell period but with outbreaks of bobbing which lasted for a few cycles at a resonant period (about 40 s), which agreed well with the predictions of a numerical finite element model. The roll response occurred mainly at a long resonant period (40–50 s), which again agreed well with the model, but there was also a significant response at ocean wave periods (5–20 s), which exceeded predictions. The strain response had a component at very long periods, which is unexplained by theory, while the surface strain at ocean wave periods agreed with the simple analytical model of Goodman et al. (1980). Using this model it is possible to predict a wave height and period that will cause breakup of the icebergs, and we conclude that swell-induced breakup is likely to occur during major storms in the open southern ocean.

INTRODUCTION

During the austral summer of 1980–1981 experiments were carried out from HMS *Endurance* on the response of Antarctic tabular icebergs to ocean wave action. The motive was an observation [*Hult and Ostrander*, 1974] that icebergs in the open southern ocean tend to be much smaller than those seen within the shelter of the Antarctic pack ice, suggesting that wave-induced flexural failure may be an important mechanism in iceberg decay. Observations of the flexural response of an arctic ice island to wave action [*Goodman et al.*, 1980], theoretical models of iceberg behavior in a seaway [*Squire*, 1981; *Kristensen and Squire*, 1983*a*], and strain data from automatic stations deployed by the 1979 Norwegian Antarctic Research Expedition [*Orheim*, 1980; *Kristensen and Squire*, 1983*b*] also point to this mechanism as being important in regions where swell of long period and large amplitude is found. This may have serious implications for attempts to develop iceberg-towing technology [*Weeks and Mellor*, 1978].

Three icebergs were studied during 1980–1981, and preliminary reports on the experiments have been given by *Kristensen et al.* [1981] and *Orheim et al.* [1982]. In this paper we give a full account of the observed flexural and body responses of the bergs to the wave field. A second season of experimental work was carried out during the 1981–1982 summer, during which two further icebergs were studied [*Kristensen et al.*, 1982]. A full analysis of the second season's data will be given in a later paper.

EXPERIMENTAL TECHNIQUE

Suitable icebergs for the experiments had to be of simple tabular shape, relatively free of obvious crevasses, and at least 400 m in linear dimension to minimize the risk of capsizing. When an experimental iceberg was found, a Waverider buoy was launched from the ship several kilometers from the iceberg to avoid diffraction effects from wave components coming from behind the berg. The Waverider was attached by a floating line to a buoy equipped with a radar reflector to reduce the chance of loss and transmitted data to a receiver and chart recorder aboard ship. Meanwhile, the experimenters and their equipment were transferred by the ship's Wasp helicopters to the iceberg where they established a station as near as possible to the geometric center of the berg's surface and laid out markers to facilitate an aerial survey of the berg.

At the center station a Schaevitz vertical accelerometer was used to measure the heave of the berg, and a manual tiltmeter, read every 2 s, was used to measure tilt along two orthogonal axes sequentially. Rotation was measured using the directional part of an Aanderaa RCM-4 current meter. Surface strain variations were measured along three axes at 120° to one another using wire strainmeters developed at Scott Polar Research Institute (SPRI) [*Moore and Wadhams*, 1980]. To set up the strainmeters, it was necessary to dig down 1–2 m through the surface snow layer, then use long (1.3 m) tubes inserted in holes drilled vertically into the firn to anchor the end units of the strainmeters. The surface material consisted of thin layers of pure ice alternating with thicker layers of firn (Figure 4), so that the conventional strainmeter mounting system of short coach bolts was not feasible. It is assumed that when the iceberg flexes, this surface material, although it has little strength, is strained in the same way as if it were the extreme fibre of a uniform thick plate.

On each of the bergs a Norwegian-built automatic station was left behind. Two of these transmitted position via the Argos satellite system and were used to plot the subsequent track of the bergs [*Vinje*, 1980]. The third was a data collection platform which transmitted heading, tilt, surface strain, meteorological parameters, and position via the Argos system. This platform failed soon after deployment except for sending position data.

While the experiments were in progress on the iceberg, a survey of the berg's shape, size, and thickness was carried out from one of the Wasp helicopters which was equipped with the

Paper number 3C0570.
0148-0227/83/003C-0570$05.00

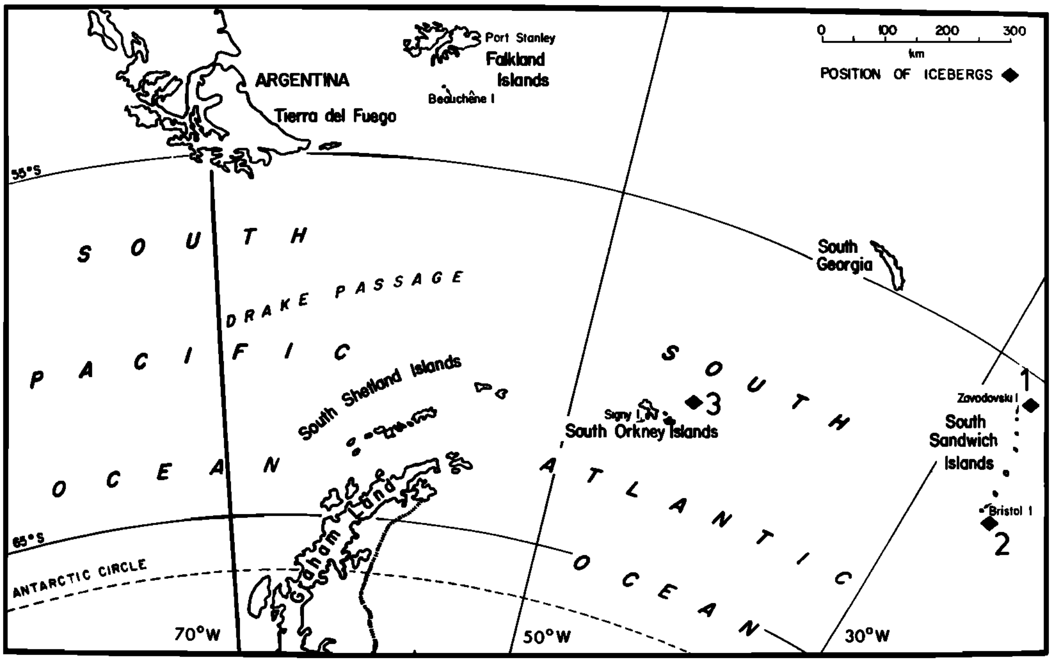

Fig. 1. A map of the South Atlantic showing the positions of the three icebergs studied.

SPRI Mark IV 60-MHz radio echo sounder [*Evans and Smith*, 1969; *Robin et al.*, 1969]. The sounder has a bandwidth of 10 MHz, a pulse length of 0.25 μs, and an accuracy of $\pm 1.5\%$. It was operated from the rear seat of the helicopter in a similar fashion to earlier surveys in the Antarctic [*Orheim*, 1980] and Svalbard [*Drewry et al.*, 1980] with a dipole antenna fitted to a wheel strut. The radio echo record was displayed on a recording oscilloscope in 'Z' mode (ice thickness versus aircraft position) and recorded by photography.

PHYSICAL CHARACTERISTICS OF THE ICEBERGS

The first iceberg to be studied (January 7, 1981) was found at 56°13'S, 27°14'W, some 20 km east of Zavodovski Island in the South Sandwich Islands (Figure 1). It was approximately semicircular in shape with dimensions of 3400 × 1800 m and a 43-m freeboard (Figure 2). Figure 3*a* is a photograph of the berg which shows that it was heavily crevassed around the edges. It appeared to be sound at the center, but on digging sample pits a closely spaced pattern of crevasses was found. Figure 4*a* shows the stratigraphy of the near-surface part of the berg. The surface snow was coarse and wet and at the melting point; its density of 520 kg m^{-3} is greater than the range of 350–420 kg m^{-3} typical of Antarctic ice shelves [*Bentley et al.*, 1964] and is more typical of ice shelf densities at about 10-m depth, suggesting that densification through melting and percolation has taken place (this effect was also observed by *Orheim* [1980]). Successful measurements were made on this berg with a single strainmeter and a heave accelerometer. Unfortunately, the recording was done only on a chart recorder rather than on the digital data logger used subsequently; the chart records were lost from the office of one of the authors (MK) prior to digitization and have not been traced. No results can therefore be reported from this iceberg. Most of the heave data from the other icebergs was also lost.

The second iceberg was found on January 11, 1981, at 58°55'S, 26°06'W, 27 km off Bristol Island (Figure 1). It was shaped like a grand piano (Figures 2*b* and 3*b*) with extreme dimensions of 1100 × 500 m. The freeboard at the center was 40 ± 2 m, measured with a Paulin altimeter. Radio echo sounding gave poor results on this berg, and a good echo could only be obtained by landing on the berg center, yielding a spot value of 237 m. This is thought to be reliable since it agrees well with

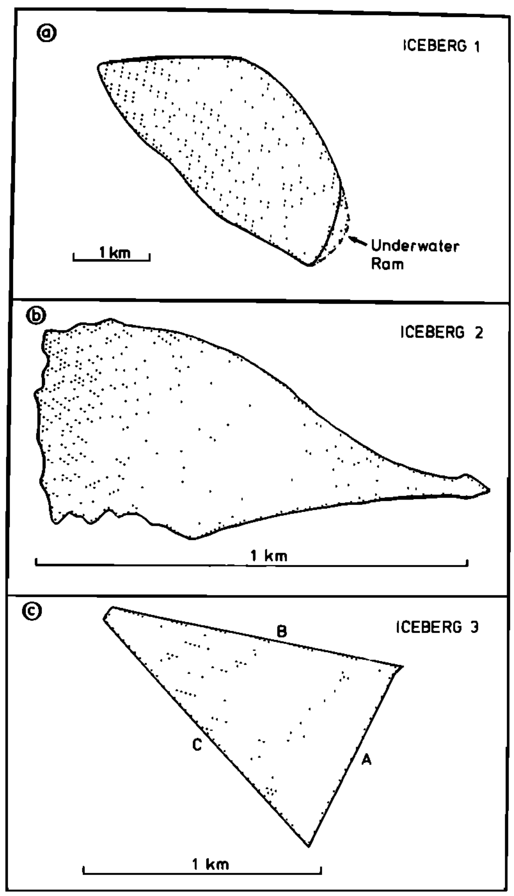

Fig. 2. Plans of the three icebergs, derived from vertical photographs taken by the ship's helicopter.

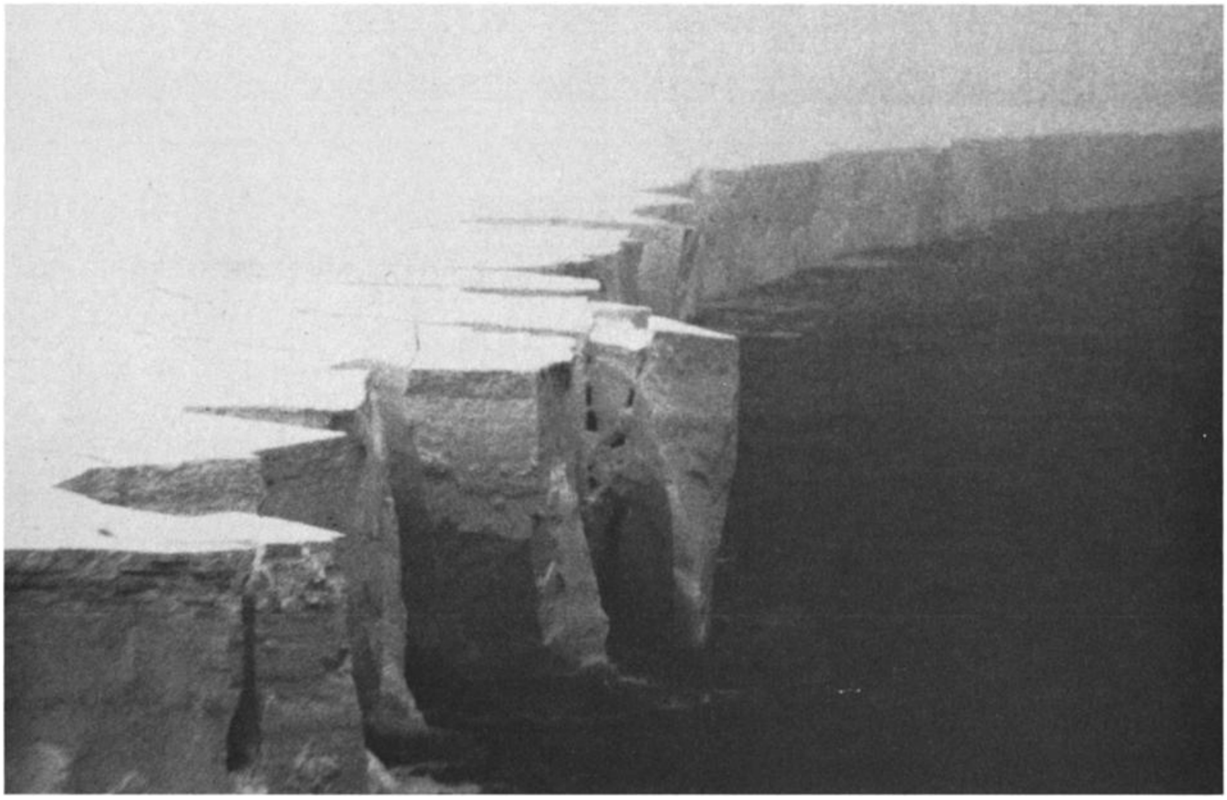

Fig. 3*a*

Fig. 3. Oblique aerial photographs of the three icebergs. (*a*) Iceberg 1; note large crevasses around edges, enlarging into ice caves. (*b*) Iceberg 2; note waves breaking against weather side of berg and lower sea state to leeward. (*c*) Iceberg 3; note wave-eroded cut around waterline.

Fig. 3*b*

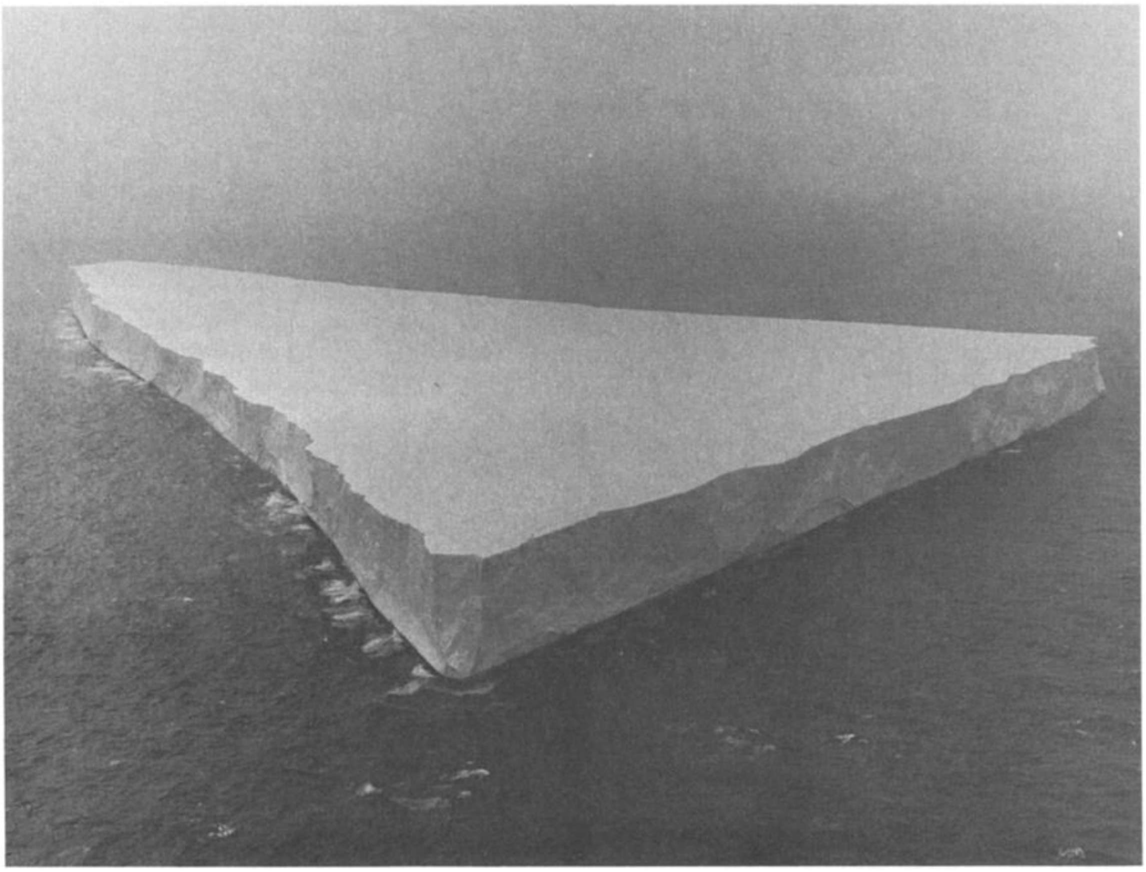

Fig. 3c

the freeboard/thickness ratios proposed by *Weeks and Mellor* [1978, Figure 20] and *Orheim* [1980]. The berg was free of visible crevasses, but its surface snow structure resembled that of the first berg. A rosette of three strainmeters was deployed, heave was measured, and two sets of orthogonal tilt measurements made. The experimenters were forced to remain overnight on this berg because of fog, so lengthy records of rotation were obtained.

The third iceberg was found on January 14, 1981, at 60°01′S, 43°15′W, near the South Orkney Islands (Figure 1). It was triangular in shape (Figure 2c) with sides of 850 m (side A), 1210 m (side B), and 1280 m (side C). The sides were straight and clear-cut (Figure 3c) and gave the appearance of having recently calved. The presence of a second iceberg of similar appearance only 3 km away was strong evidence that a larger berg had recently broken up. The surface snow on the berg contained ice layering similar to the earlier bergs (Figure 4c), but the snow was drier and firmer, supporting the weight of the experimenters, while on icebergs 1 and 2 they sank to their thighs. The freeboard of the berg was greater at its ends than in the center (Figure 5). Radio echo sounding yielded clear signals. Twelve transects were carried out, and Figure 6 shows a con-

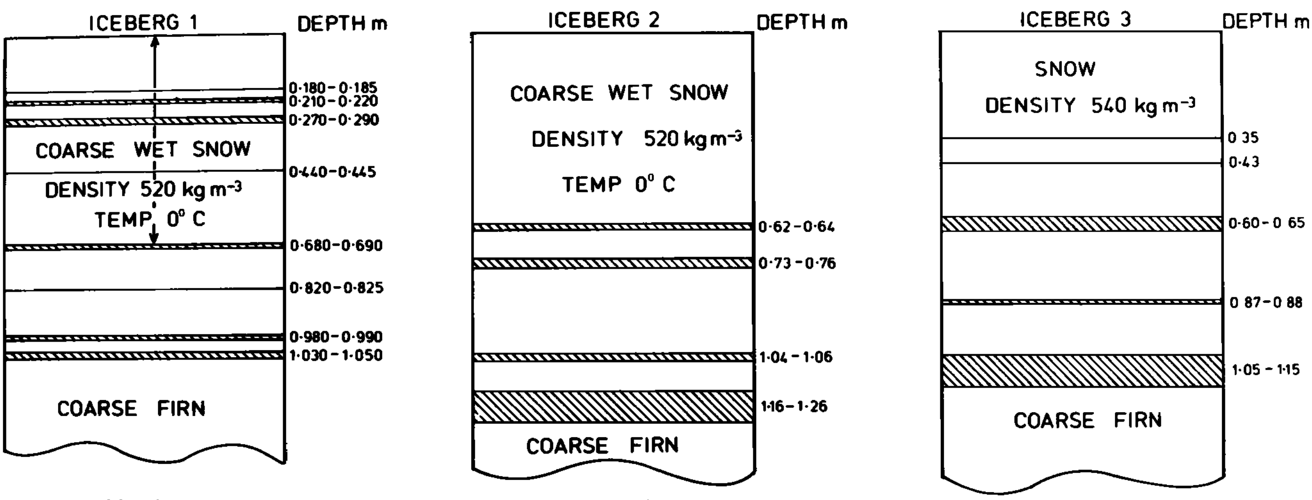

Fig. 4a Fig. 4b Fig. 4c

Fig. 4. Stratigraphy of uppermost 2 m of iceberg surfaces, showing positions of thin ice layers in the snow and firn.

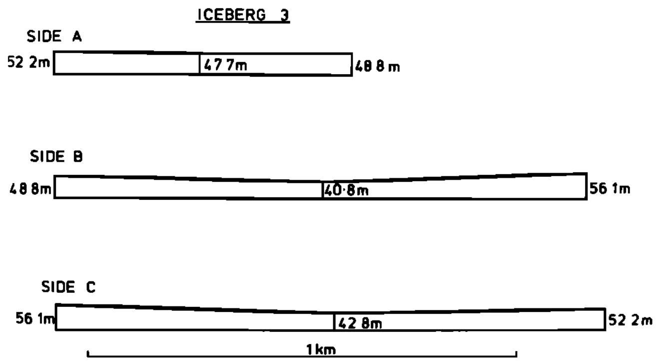

Fig. 5. Observations of the freeboard of iceberg 3.

tour map of the berg thickness constructed from these transects. The mean ice thickness was 297 m, with a standard deviation of 23 m and a tendency toward a lower draft under the center of the berg than under the ends, thus giving approximate isostatic compensation for the freeboard. A rosette of three strainmeters was deployed on the berg, and all the data were successfully recovered from the tape record. A pair of tilt measurements was also taken.

Ocean Wave Spectra

The Waverider buoy yields a one-dimensional spectrum with no information on directionality. In future operations it is hoped to use a directional wave buoy, since the body response of a irregular iceberg depends on the direction from which waves approach it. Figure 7 shows six spectra recorded on January 11, at half-hour intervals, representing the development of the sea during the period of the experiments on iceberg 2. There are two main components to the spectrum: a local wind-generated sea with a peak at about 7-s period; and a swell which gradually decreased in peak period from 12.9 to 10.6 s during the 3 hours of recording. As Figure 8 shows, the rate of increase of the frequency of the swell peak (df/dt) is approximately constant. This occurs when swell is coming from a well-defined generating area, at a distance S given by

$$df/dt = g/2\pi S \tag{1}$$

[*Barber and Ursell*, 1948; *Munk et al.*, 1963]. The line of best fit to the data in Figure 8 gives a distance of 840 km, and a storm which began 11 hours 40 min before the first recording, i.e., at approximately 0001 UT on January 11.

Figure 9 shows four spectra covering the period of the experiments on iceberg 3. Again there are two main components to the spectrum, both of shorter period than for iceberg 2. The swell, which dominates in energy, is of period 10 s, again showing an increase in frequency during the experiment, while the local wind sea is of 5-s period.

Heave Response

The only heave record not to be lost was a short section of the chart record from iceberg 2. Figure 10 shows this record, which was, however, characteristic of the iceberg's behavior throughout the experiment. The heave of the berg alternated between a response to the swell component of the sea, at about 13-s period, and a breaking-out into a higher-amplitude, longer-period heave response at about 36-s period. This long-period heave would typically last for about six cycles before subsiding into a simpler 13-s swell response. Figure 11 is an energy spectrum of the heave data. The short record length means that the spectrum is very approximate, with a standard error of $\pm 58\%$ in each energy value, but it clearly shows the two characteristic responses. There is no doubt that the short-period heave is a response to the swell, while the long-period heave is a resonant bobbing of the berg in the water. The spectral analysis gives this resonant period of vertical oscillation as 36 ± 5 s.

The bobbing period for a body with vertical side walls and uniform draft h_i is given by

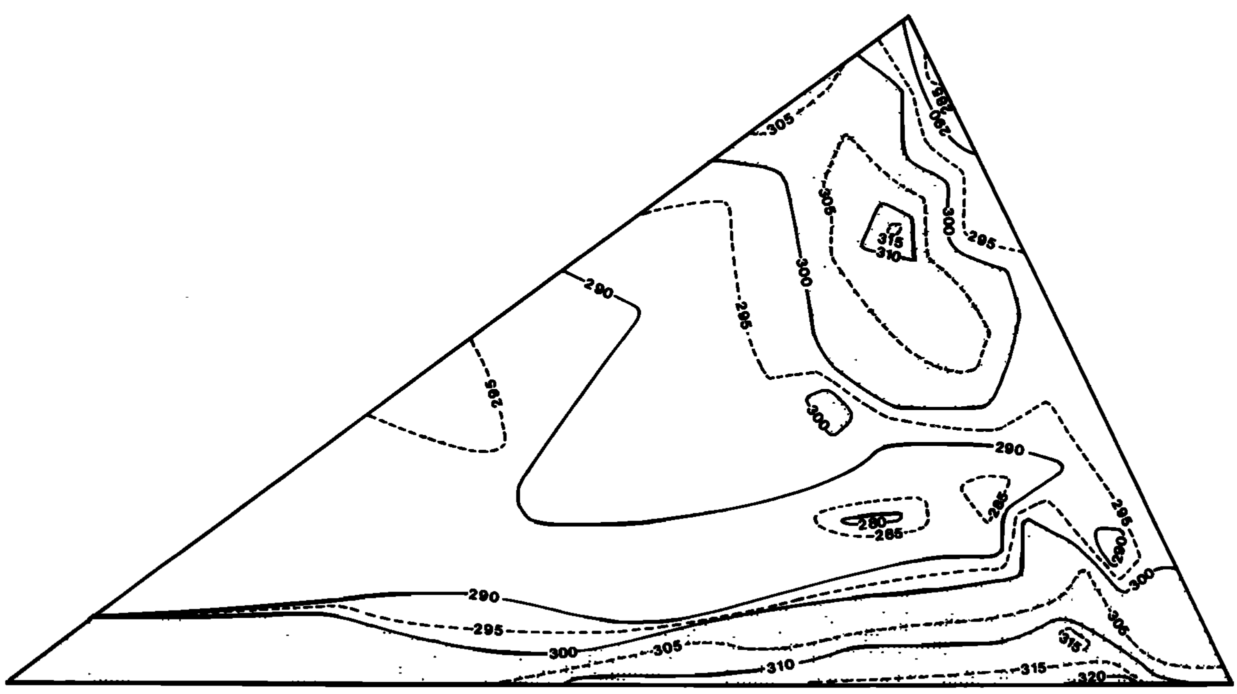

Fig. 6. Contour map of the thickness of iceberg 3, constructed from the results of 12 radio echo transects. Thicknesses are in meters; areas thicker than 300 m are shaded.

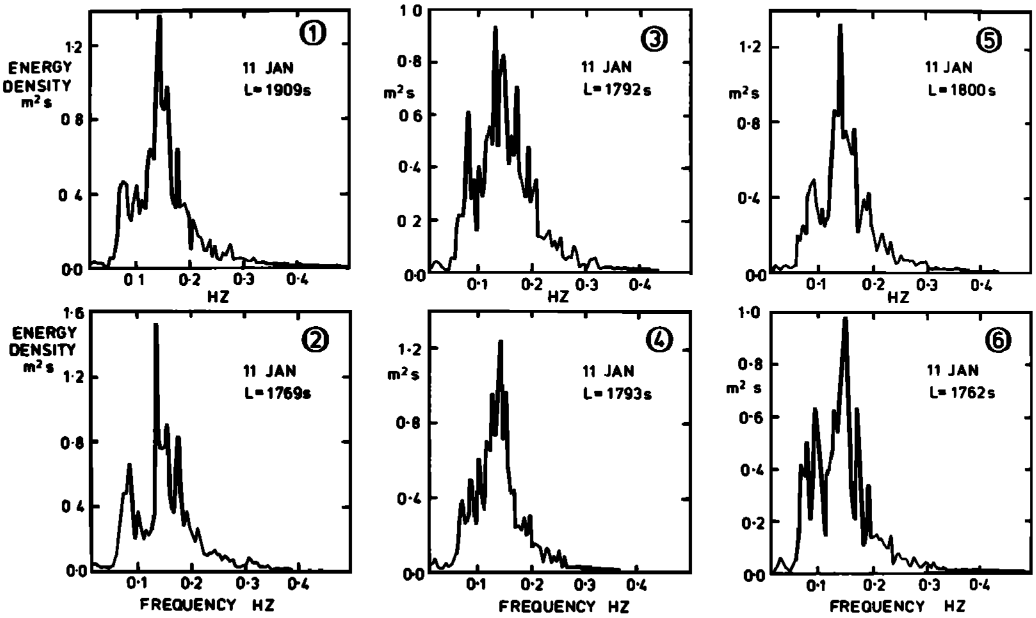

Fig. 7. One-dimensional ocean wave spectra recorded during experiments on iceberg 2.

$$T_b = 2\pi(h_i/g)^{1/2} \quad (2)$$

if we neglect added mass and damping coefficient. This predicts a T_b of 28.2 s for the observed draft of 197 m. A more sophisticated numerical analysis [*Squire*, 1981], which takes account of the inertia of the water displaced by the bobbing, gives 40 ± 3 s as the period at which the response amplitude operator (RAO) of the iceberg is greatest in bobbing. The RAO is the amplitude of response on the assumption of a monotonic incident wave of unit amplitude, and therefore the RAO peak period can be identified with the bobbing period so long as the incident spectrum is flat. If, as normally occurs, the spectral energy density decreases rapidly with increasing wave period, then the bobbing period may be slightly lower than the RAO peak. Theory and observation therefore agree well in this case.

The Waverider cannot reliably measure energy at periods beyond 20 s, so the energy input from the sea at long periods is unknown. In general, such measurements are difficult because of interference from the overwhelmingly greater energies at short periods and because of the decline in response of accelerometer buoys. Most successful techniques depend on removing shorter period waves, for example, by the use of seabed pressure transducers. Recently, strainmeter measurements on the central arctic ice cover from the Fram 3 station [*Manley et al.*, 1982] have revealed 30-s waves with 3-mm amplitude, the pack ice in this case having filtered out the shorter components. The bobbing energy occurring in Figure 10 involves an amplitude of approximately 1.5 cm which, at a peak RAO of 1.822 computed using *Squire* [1981], is equivalent to an ocean wave amplitude of 8.2 mm. This value is within the range of possibility suggested by the Arctic Ocean strain results. Thus it appears that the very small amount of energy present in the sea at long periods (around 40 s) is the cause of the most energetic component of heave response in icebergs.

Theoretical treatment of long-period waves [e.g., *Larsen*, 1978*a*, *b*, 1979] shows that packets of gravity waves at normal wind wave periods can force a fluid motion on the length scale of the modulation envelope. These forced long waves have an amplitude which increases as the depth decreases and which depends on the depth parameter kD (D is water depth and $k = 2\pi/\lambda$, where λ is wavelength). When $kD > 1.363$, the forced waves move in the same direction as the originating wave packets and are called 'envelope solitons.' The water depths at the three iceberg sites (approximately 600, 800, and 5000 m for bergs 1, 2, and 3) give kD values of about 2, 3, and 15 for 35–45 s waves. Solitons can therefore be generated, with the intriguing possibility that the long-period forcing is greater when bergs are in shallow water than when they are in deep ocean basins. Since the observed long-period heave of iceberg 2 never persisted for more than about 5 min at a time, it is possible that the long-period forcing itself occurs in the form of wave packets.

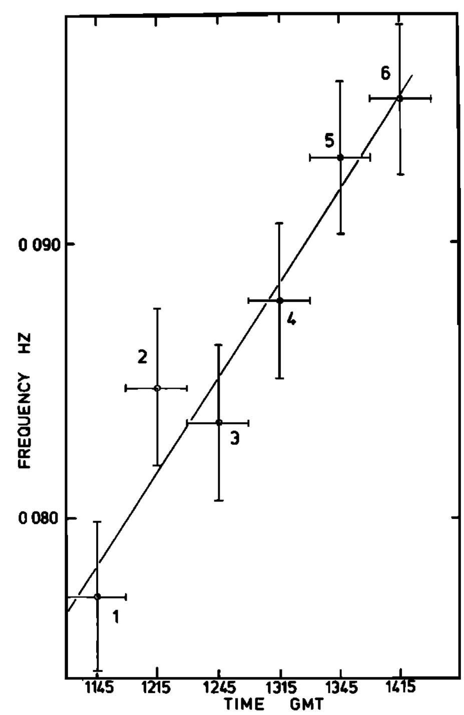

Fig. 8. Rate of change of the frequency of the swell peak in the spectra of Figure 7.

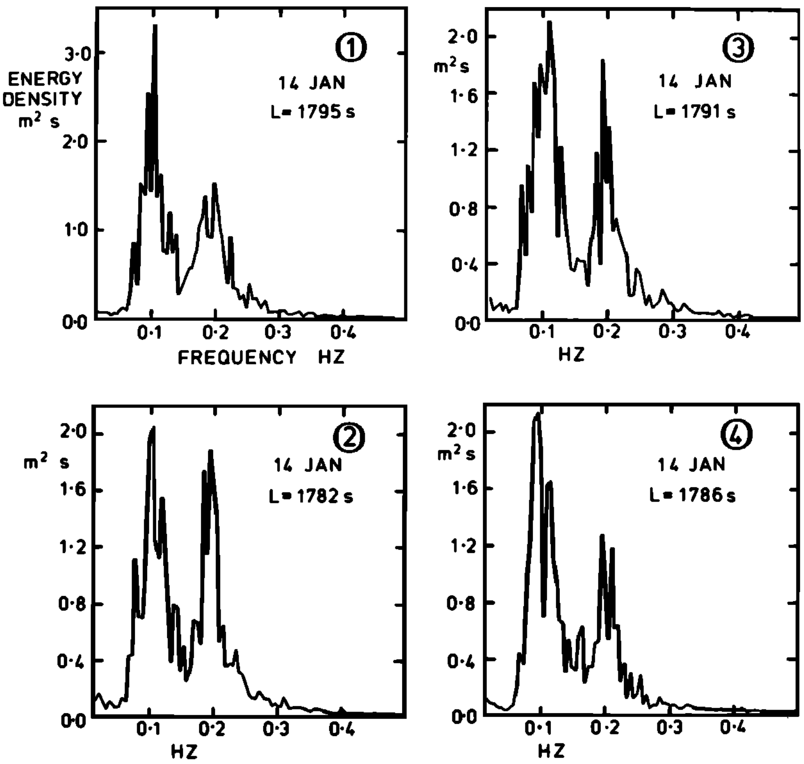

Fig. 9. Ocean wave spectra recorded during experiments on iceberg 3.

ROLL RESPONSE

Figure 12 shows the records and spectra of tilt observed on iceberg 2. 'Tilt X' measurements were made with the tiltmeter oriented along the major axis of the iceberg, and 'tilt Y' measurements were orthogonal to this. During the first set of recordings the tilt X energy was evenly divided between a very long period response and a response at approximately the swell period, while for tilt Y a very long period response was dominant. During the second set of measurements the long-period response became dominant along the X axis, while the swell response dominated along the Y axis. During the 6-hour interval between the two sets of measurements the iceberg rotated through 135° so that the change in energy partition may have been due to the change in the orientation of the iceberg relative to incoming wave trains. The periods of the spectral peaks in Figure 12 are given in Table 1. The figures suggest that the long-period response has a slightly different frequency for the two axes of roll.

Again we interpret this long-period response as being the natural resonant roll period of the iceberg. A formula for the roll period of a homogeneous rectangular tabular iceberg about its center of gravity, neglecting added mass and damping coefficient, is given by *Foldvik et al.* [1980*a*] as

$$T_r = 2\pi\left[\frac{\alpha h(L^2 + h^2)}{g(L^2 - 6\alpha(1-\alpha)h^2)}\right]^{1/2} \tag{3}$$

where h is thickness of the berg, L is length of the berg orthogonal to the axis of roll, and $\alpha = \bar{\rho}_i/\bar{\rho}_w$, where $\bar{\rho}_i$ is mean density of ice in the berg and $\bar{\rho}_w$ is mean density of seawater from depth 0 to h_i in the water column.

We can use 1.03 for $\bar{\rho}_w$, while *Weeks and Mellor* [1978] recommend for $\bar{\rho}_i$ the empirical relation

$$\bar{\rho}_i = 0.91\ (1 - 16/h) \tag{4}$$

with h in m. Substituting 1100 and 500 m as the two lengths gives 34.6 and 29.4 s as the periods for tilt Y and tilt X, respectively. These are subject to a small correction owing to the fact that the center of roll lies above the center of gravity. A much greater change in T_r occurs if we apply the numerical model of *Squire* [1981], which predicts 40 ± 3 s as the RAO peak period for tilt X and 45 ± 3 s for tilt Y, assuming a rectangular iceberg facing a beam sea. The predicted values show good agreement with the observations.

The nature of the roll response through the frequency range in which the Waverider is sensitive was examined by computing the frequency response function [*Bendat and Piersol*, 1971]

$$H(f) = G_{12}(f)/G_1(f) \tag{5}$$

where $G_1(f)$ is the spectral density of the input (wave record) at frequency f and $G_{12}(f)$ is the cross-spectral density between input and output (concurrent tilt). The $|H(f)|$ is then the gain factor, equivalent to a ratio of amplitudes; the phase factor arg $H(f)$ is meaningless because of the unknown physical separa-

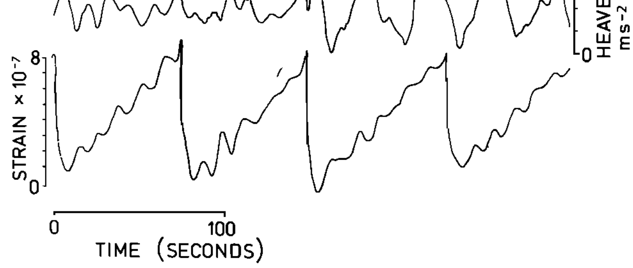

Fig. 10. Concurrent heave and strain recordings from iceberg 2. The heave can be seen breaking out into a long-period bobbing response. The strain record is modulated by a sawtooth due to thermal drift and instrument rezeroing.

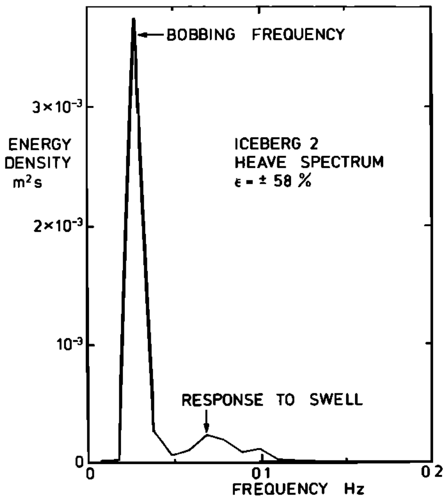

Fig. 11. Energy spectrum of heave from iceberg 2.

tion between Waverider and iceberg station. Figure 13 shows the results, compared with the predictions of the numerical theory of *Squire* [1981], as modified [*Kristensen and Squire*, 1983*a*] to allow for the variation of density with depth through the iceberg. In this frequency range the numerical theory appears to be seriously deficient; it predicts a falloff in roll response with increasing frequency which is much more rapid than that observed. The valid range for comparison extends from the Nyquist frequency of 0.25 Hz (due to the 2-s sampling interval for tilt), to a low-frequency limit of 0.05 Hz below which the Waverider response falls off. Throughout this range the theory underestimates the roll response by at least an order of magnitude. A possible explanation is that the theory neglects damping due to turbulence of the displaced water; the effect of viscous damping is to flatten the long-period resonant peak and to make the falloff in response at increasing frequency a more gentle process.

TABLE 1. Periods of Spectral Peaks in Figure 12

	Long-Period Peak, s	Swell Response, s
Tilt X	37 ± 9	14.2 ± 1.9
Tilt $X2$	37 ± 3	14.4 ± 0.7
Tilt Y	44 ± 8	14.7 ± 0.8
Tilt $Y2$	43 ± 4	15.3 ± 0.5

Figure 14 shows the records and spectra of tilt observed on iceberg 3. Once again the long-period resonant rolling is dominant in the energy spectrum. It occurs at a period of 56 ± 8 s for tilt X and 76 ± 20 s for tilt Y. In the case of tilt Y the resonant response is so regular that a better frequency estimate can be made by counting cycles; this yields 65 s. For tilt X the tiltmeter was oriented along the major axis of the iceberg, bisecting the angle between sides B and C (Figure 2*c*); tilt Y was orthog-

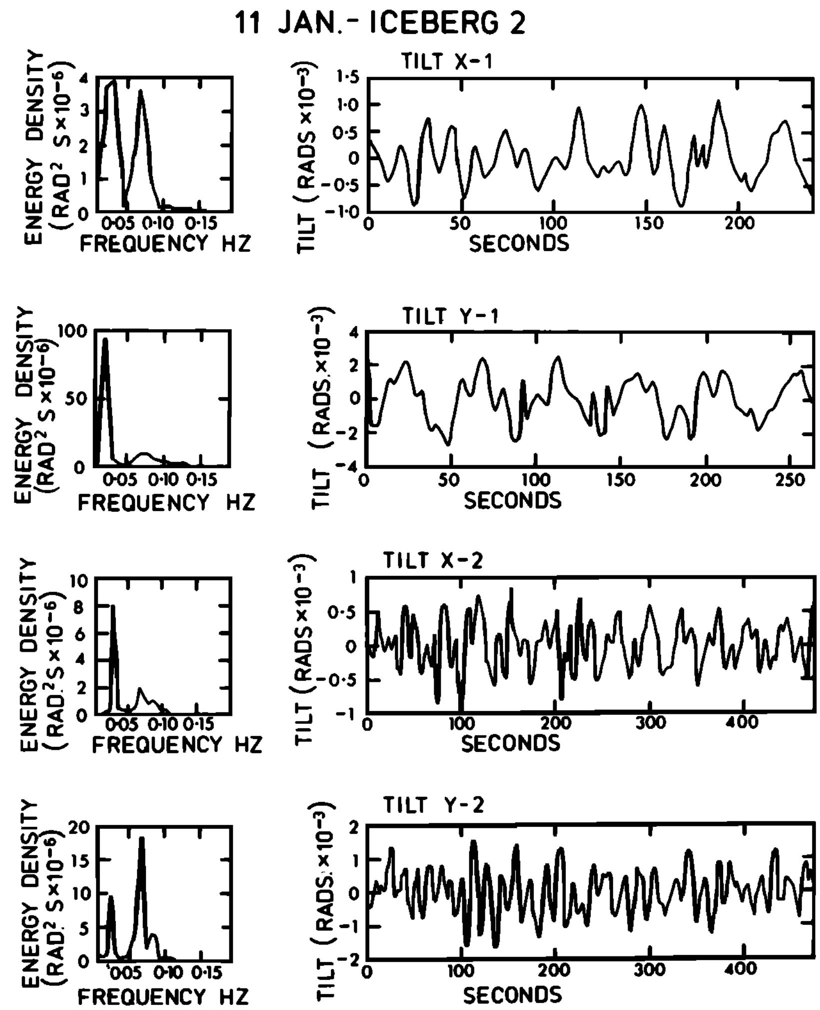

Fig. 12. Records and energy spectra of roll from iceberg 2. Standard error in energy values ±58%.

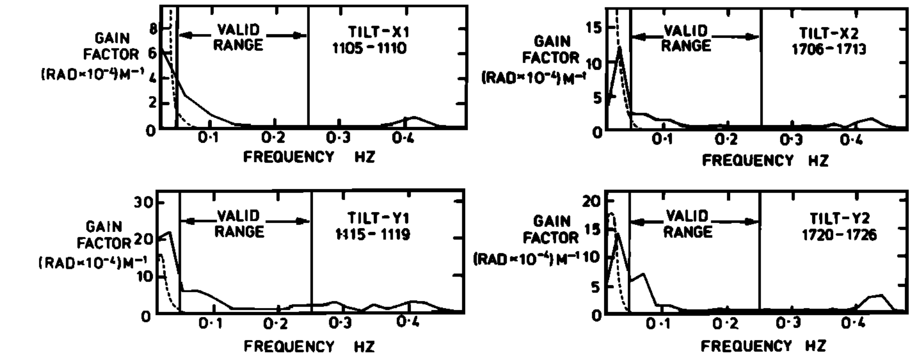

Fig. 13. Gain factor of roll response for iceberg 2, with theoretical predictions of *Squire* [1981] model added as dotted lines.

onal to this. Simulations using *Squire* [1981] give 52 ± 2 s and 51 ± 1 s for the RAO peak periods of tilt X and tilt Y, respectively, while the less accurate equation (3) yields 35.6 and 33.7 s. In both cases the iceberg is assumed to be rectangular rather than triangular, with dimensions of 1200 × 850 m and a thickness of 300 m. The discrepancy between observation and the numerical theory is not great and may be due to the simplified shape employed in the theory. In Figure 14 the spectrum has been plotted on a logarithmic as well as a linear scale of energy, and it can be seen that apart from the major peaks the energy varies with frequency approximately as a negative exponential.

Figure 15 shows the gain factor for the roll response on iceberg 3, compared with simulations using *Kristensen and Squire* [1983*a*]. Again the observed response at normal ocean wave frequencies is greater and falls off more slowly with increasing frequency than the theoretical response.

Finally, we note that if the experimental sites are not directly over the center of mass of each berg, the roll is able to make a contribution to the apparent heave response. Fortunately, a comparison of observed magnitudes shows that the error in positioning would have to be at least 1 km before the observed roll could be a significant component of the observed heave.

STRAIN RESPONSE

Figure 16 shows the corrected records and energy spectra of strain from two strainmeters on iceberg 2 (the third strainmeter failed to operate); the energies have a standard error of ±33%. Part of a raw strain record is shown in Figure 10 alongside a concurrent heave record. The sawtooth waveform represents thermal drift and automatic rezeroing, which were removed in processing to generate Figure 16. Figure 10 shows that when the berg broke out into an interval of resonant bobbing there was no apparent change in the strain record, which continued to be mainly a response at the swell period. Nevertheless, the spectra show a component of strain energy at very long period, although it is not dominant in the same way as the long-period tilt or heave responses. The peaks of the spectra occur at 50 ± 8 s and 13.0 ± 0.7 s for strainmeter 2 and 48 ± 4 s and 13.9 ± 0.5 s for strainmeter 3.

The very long period response does not occur in either numerical [*Squire*, 1981] or analytical simulations. A simple analytical approximation for the strain at the center of an iceberg or ice floe was developed by *Goodman et al.* [1980]. The simplifying assumptions, which are described more fully by

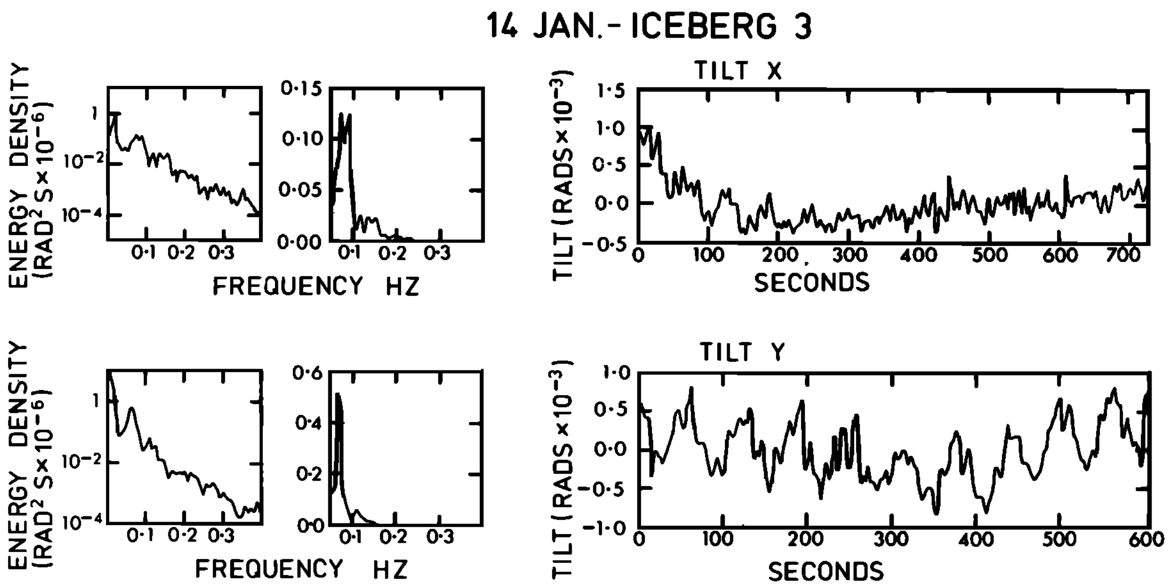

Fig. 14. Records and energy spectra of roll from iceberg 3. Standard error in energy values ±45%. The energies are plotted in logarithmic and linear forms.

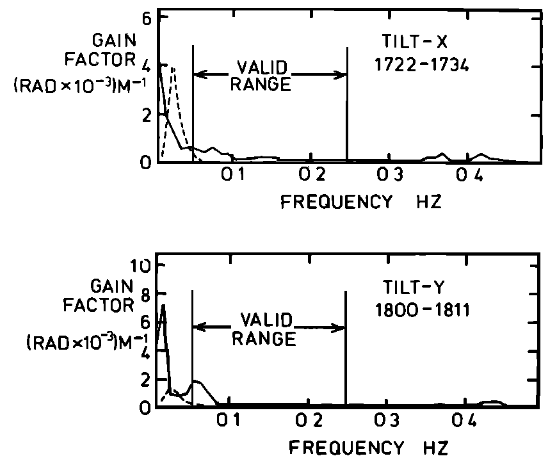

Fig. 15. Gain factor of roll response for iceberg 3 with theoretical predictions added as dotted lines.

Wadhams [1983], include setting the added mass and damping coefficient of the berg to zero, adopting the Froude-Krylov hypothesis (i.e., ignoring the potential due to wave diffraction by the iceberg) and neglecting the hydrodynamic effect of the vertical sidewalls. Figure 17 shows the result of using this model to calculate the strain along the major and minor axes of rectangular icebergs with extreme dimensions equal to those of icebergs 2 and 3. Incoming waves are assumed to be oriented parallel to the axis along which the strain is being computed. The theoretical strain response of iceberg 2 at 50-s period is only of order 10^{-7} m^{-1}, which together with the observed strain amplitude of about 0.2×10^{-6} implies a wave height of some 4 m at that period, which was certainly not seen. Therefore we cannot explain the observed long-period strain in terms of a simple bending response to long-period energy in the ocean. A proper explanation probably involves a nonlinear interaction whereby one of the other resonant responses of the iceberg (such as tilt) causes a strain field to be induced in the berg.

The strain response of iceberg 2 at normal wave periods was examined by computing the gain factor (Figure 18). The valid range for comparison extends from 0.05 Hz, the lowest frequency at which the Waverider responds well, to 0.5 Hz, the Nyquist frequency for the data logger. In the absence of a full rosette it is not possible to ascertain the direction of the principal strain in iceberg 2. The two gain factors of Figure 18 are therefore both underestimates of the true strain response, since each represents a strain vector in a direction other than that of

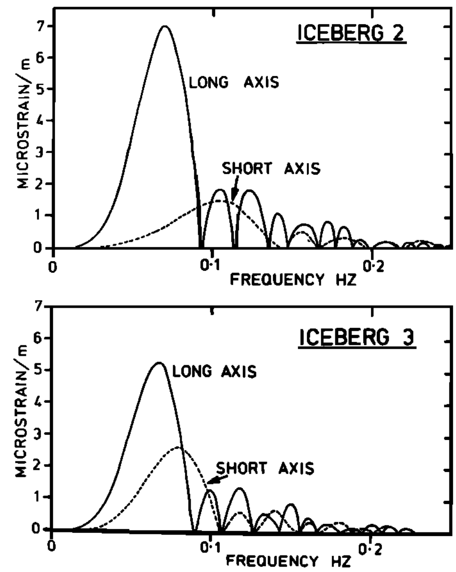

Fig. 17. Theoretical strain response of icebergs 2 and 3 along long and short axes. The model uses rectangular icebergs of same extreme dimensions as icebergs 2 and 3 and assumes that waves are incident along direction in which strain is measured.

the incoming wave energy. In setting up the array, strainmeter 2 was oriented within 7° of the longest axis of the iceberg, defined by survey flags. Strainmeter 3 lay at 58° to the longest axis and therefore recorded more of the cross-axis strain component. Thus, if wave energy were all incident along the longest axis of the iceberg, the gain factor for strainmeter 2 ought to match the theoretical strain response for the long axis case in Figure 17. In fact, as can be seen by a comparison of the two figures, the observed gain factors are of the correct order of magnitude and display some of the features of the theoretical curves. In view of the irregular shape of the iceberg and the uncertainties in wave and strain directions, better agreement cannot be expected.

Data from a full rosette of three strainmeters were recovered from iceberg 3, which thus provide the best test of the theoretical model. Figure 19 shows the corrected records and energy spectra of strain from this iceberg. The strains again show mainly a response at swell frequencies but with some very long period energy present. The two main peaks of each spectrum occurred at the following periods: strainmeter 1, long-period peak 64.0 s, swell peak 15.6 s; strainmeter 2, long-period peak 89.0 s, swell peak 14.6 s; strainmeter 3, long-period peak 49.9 s, swell peak 15.6 s. The periods of the long-period peaks are

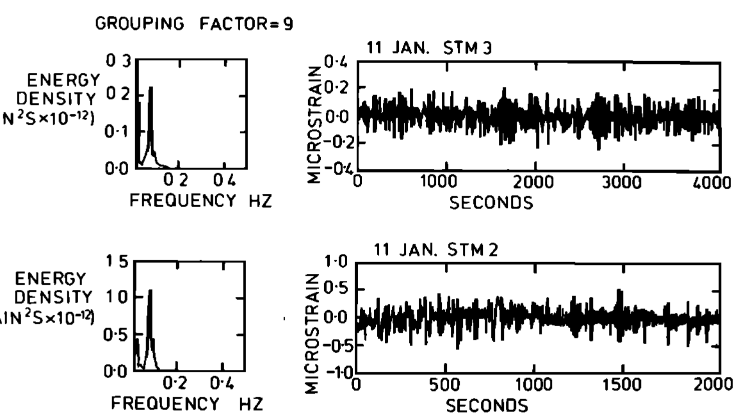

Fig. 16. Corrected records and energy spectra of strain from two strainmeters on iceberg 2.

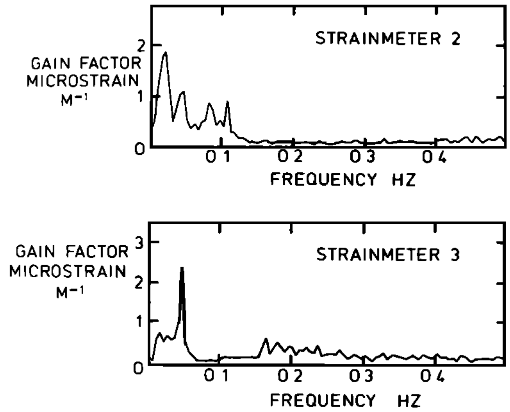

Fig. 18. Gain factor of strain response for strainmeters 2 and 3 on iceberg 2.

subject to large statistical error because of the frequency grouping used in the analysis.

A rosette analysis for principal strains [*Squire*, 1978] was carried out on the records. This technique yields the maximum principal strain amplitudes as a function of frequency, together with the angle between the direction of the principal strain and the orientation of strainmeter 1. It also yields the minimum principal strain, i.e., the strain amplitude at right angles to the major strain direction. A high ratio of maximum to minimum principal strain indicates a strain response to an almost unidirectional incident wave field. When divided by the square root of the energy components in the Waverider energy spectrum, the result is a normalized gain factor curve that is equivalent to Figure 18 but better in that the strain response is always measured in the direction of maximum strain.

Figure 20 shows the result of this principal strain analysis. Throughout the valid frequency range (0.05–0.5 Hz) the principal strains are in a direction about 20°–30° anticlockwise from strainmeter 1. On the iceberg strainmeter 2 was oriented in the direction of the major axis (a line bisecting the angle between sides B and C in Figure 2c), with strainmeter 1 at 120° anticlockwise from it. The principal strain directions therefore

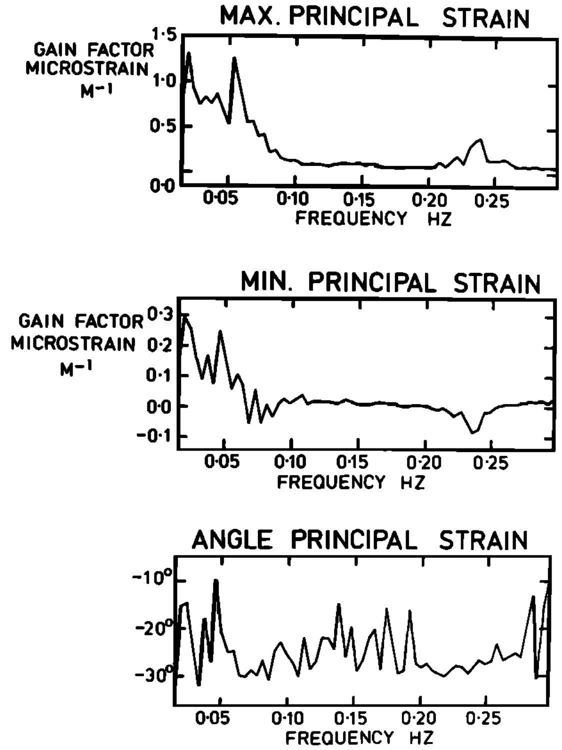

Fig. 20. Result of principal strain analysis on iceberg 3. (top) Gain factor for maximum principal strain, i.e., the strain response in the direction from which maximum wave energy is coming. (middle) Gain factor for minimum principal strain, i.e., strain response along orthogonal axis to maximum principal strain. (bottom) Angle between maximum principal strain direction and strainmeter 1, measured clockwise from strainmeter.

lie at 30°–40° to the major axis, i.e., approximately parallel to side C. We thus expect the gain factor for principal strain to correspond approximately with the 'long axis' theoretical analysis of Figure 17 for iceberg 3. It clearly corresponds quite well. The peak response occurs at about the same frequency (0.06 Hz) and is of the same order of magnitude (1.4×10^{-6} compared with 5×10^{-6} for theory). It falls off with increasing

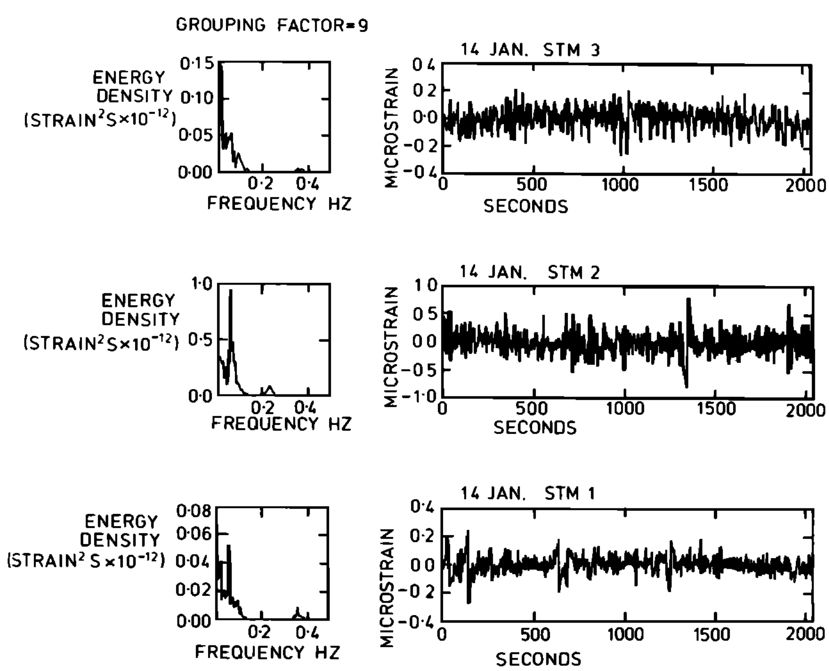

Fig. 19. Corrected records and energy spectra of strain from strainmeter rosette on iceberg 3.

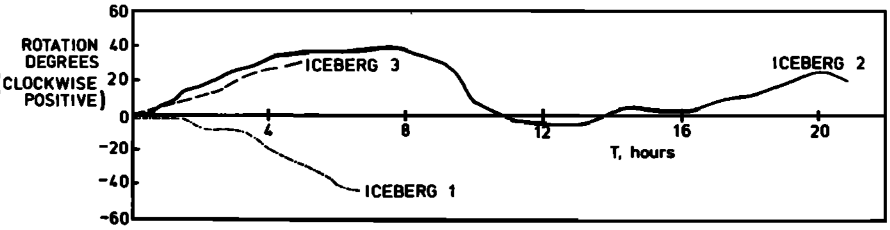

Fig. 21. Rotation of the three icebergs.

frequency in the same way, reaching a near-zero value (probably the noise level) at about 0.09 Hz, while the theoretical response goes to zero at 0.09 Hz. At higher frequencies the experimental gain factor is very small except for an unexplained bump at 0.24 Hz, while the theoretical gain is also very small, undergoing a number of cycles. At frequencies below 0.05 Hz the gain factor in Figure 20 is exaggerated because of the reduced Waverider response. We cannot say therefore how well the shape of the experimental and theoretical curves resemble one another at very low frequencies, although clearly at 50–80 s period there is an observable strain which greatly exceeds theoretical predictions.

The only previous test of the analytical strain model on thick ice involved a 35-m-thick Arctic ice island [*Goodman et al.*, 1980], although it has been shown to work well for sea ice (D. J. Goodman et al., manuscript in preparation, 1983). Its success in giving a good fit to the observed strain response of thick (240 and 300 m) icebergs is surprising in view of the approximations and assumptions involved, but gratifying in that it provides us with a simple analytical equation which can be used to predict iceberg strain response in a seaway. The main drawback of the theory is its complete failure to predict the observed long-period response, which appears to occur near the resonant tilt frequency. Further theoretical analysis of the interaction between body and flexural responses is needed to solve this problem.

ROTATION OF THE ICEBERGS

Figure 21 shows the results of the rotation measurements on the three icebergs. Of these, iceberg 2 was measured through a complete cycle, which had not been achieved in earlier observations [*Foldvik et al.*, 1980*b*] although long-term records from automatic stations are now under analysis by one of the authors (OO). Typical rotation rates were 5°–10° per hour, although iceberg 2 at one stage exceeded 40° per hour, maintained for some 30 min. The inertial period at the latitude of iceberg 2 is 14.0 hours, and this agrees quite well with the period of the observed cycle of rotation, which had an amplitude of 22°. Models of iceberg drift assume that the main forces involved are wind and water stresses and Coriolis force, with sea surface tilt and wave radiation pressure as lesser influences. In many cases the predicted (and observed) trajectories include inertial loops [e.g., *Sodhi and El-Tahan*, 1980; *Smith and Banke*, 1981]. Such models predict only the motion of the iceberg's center of gravity and say nothing about rotation, but it is reasonable to expect that an irregular iceberg undertaking an inertial loop will also rotate due to the net moment of the unbalanced wind and water stresses acting over its surfaces. Any scheme to tow icebergs must take account of this rotational tendency.

CONCLUSIONS

The field program from HMS *Endurance* was conceived in order to test the idea that wave-induced flexural failure is an important cause of iceberg decay in the open southern ocean. On making the measurements we found to our surprise that a major component of an iceberg's response to the sea consists of long-period bobbing and rolling motions at 40–80 s period. Part of the strain response also occurs at these very long periods, which cannot be explained by current theory. We conclude that as a result of an interaction between modes of response, the tilt and/or heave can induce a flexural strain field in the berg. The magnitude of this long-period strain is such that it may be the triggering factor in wave-induced breakup.

The strain response at normal wave and swell periods agrees surprisingly well with the predictions of the simple analytical theory of *Goodman et al.* [1980]. The form of the theoretical response curves (Figure 17) is very significant as the maximum gain factor occurs at a frequency ($\sim$0.06 Hz) typical of swell from southern ocean storms. Such swell is therefore especially effective in causing large strains.

The failure strain of an iceberg is not known, since no strain measurement has been made during or near breakup. *Goodman et al.* [1980] discuss fracture mechanics theory as applied to flexural failure, which predicts that failure occurs through the uncontrolled propagation of the longest crack initially present in the iceberg. They estimated a failure strain ε_{crit} for pure ice of 2.1×10^{-4} if the largest crack is of length 1 mm (a typical grain size). A 'perfect' iceberg will certainly have many cracks longer than 1 cm, giving an ε_{crit} of 6×10^{-5} ($\varepsilon_{crit} \propto$ (crack length)$^{-1/2}$), while a crevassed iceberg (such as iceberg 1) will have cracks at the surface exceeding 10 m in length, giving an ε_{crit} of 2.1×10^{-6}. These estimates may be invalid if another mechanism such as fatigue controls flexural failure under cyclic loading, but they provide a basis for discussion.

On iceberg 3 the greatest observed strain amplitude during 33 min of recording was 0.7×10^{-6} (strainmeter 2 at 1400 s, Figure 19), while the significant wave height H_s was 1.1 m. H_s is calculated from m_0, the total energy in the spectrum, by the relation $H_s = 4\sqrt{m_0}$ [*Cartwright and Longuet-Higgins*, 1956]. Now H_s values exceeding 10 m regularly occur in the southern ocean, especially during winter [*Mognard et al.*, 1983]. Since we expect strain amplitude to vary approximately as H_s, we can say that a strain amplitude of at least 7×10^{-6} is likely during a major storm. This would be enough to fracture the iceberg so long as it had a crack longer than about 1 m in its surface. In fact, the maximum strain may well be much greater than this, since the duration of any storm will greatly exceed 33 min and since Figure 17 suggests that strain will increase faster than H_s due to the shift in the spectrum toward longer periods at higher energy levels. Our conclusion must be that typical tabular icebergs are highly susceptible to wave-induced flexural failure during storms, so that towing becomes a hazardous operation.

Acknowledgments. We are grateful to the Hydrographic Department of the Admiralty for providing the opportunity to sail aboard HMS *Endurance*, to her captain and crew for their cooperation, and to the British Petroleum Co. Ltd. for financial support. At the time of the experiments PW held the Office of Naval Research Chair of Arctic

Marine Science at the Naval Postgraduate School, Monterey, California, and is grateful for their support. MK acknowledges the support of a British Council grant.

REFERENCES

Barber, N. F., and F. Ursell, The generation and propagation of ocean waves and swell, 1, Periods and velocities, *Philos. Trans. R. Soc. London, Ser. A, 240*, 527–560, 1948.

Bendat, J. S., and A. G. Piersol, *Random Data: Analysis and Meeasurement Procedures*, 507 pp., John Wiley, New York, 1971.

Bentley, C. R., R. L. Cameron, C. Bull, K. Kojima, and A. J. Gow, Physical characteristics of the Antarctic ice sheet, *Antarctic Map Folio Ser. Folio 2*, Am. Geogr. Soc., New York, 1964.

Cartwright, D. E., and M. S. Longuet-Higgins, The statistical distribution of the maxima of a random function, *Proc. R. Soc. London, Ser. A, 237*, 212–232, 1956.

Drewry, D. J., O. Liestøl, C. S. Neal, O. Orheim, and B. Wold, Airborne radio echo sounding of glaciers in Svalbard, *Polar Rec., 20*(126), 261–266, 1980.

Evans, S., and B. M. E. Smith, A radio echo equipment for depth sounding in polar ice sheets, *J. Phys. E, 2*, 131–136, 1969.

Foldvik, A., T. Gammelsrød, and Y. Gjessing, Measurements of oscillations and flexure of icebergs, *Ann. Glaciol., 1*, 29–30, 1980*a*.

Foldvik, A., T. Gammelsrød, and Y. Gjessing, Flow around icebergs, *Ann. Glaciol., 1*, 67–70, 1980*b*.

Goodman, D. J., P. Wadhams and V. A. Squire, The flexural response of a tabular ice island to ocean swell, *Ann. Glaciol., 1*, 23–28, 1980.

Hult, J. L., and N. C. Ostrander, Applicability of ERTS to Antarctic iceberg resources, Third Earth Resources Technology Satellite-1, Symposium edited by S. C. Freden and M. A. Becker), vol. 1B, *NASA Spec. Publ., SP-251*, 1467–1490, 1974.

Kristensen, M., and V. A. Squire, Modelling of Antarctic tabular icebergs in ocean waves, *Ann. Glaciol., 4*, 152–157, 1983*a*.

Kristensen, M., and V. A. Squire, Automatic collection of tilt and strain data from Antarctic icebergs, *Ann. Glaciol., 4*, 147–151, 1983*b*.

Kristensen, M., O. Orheim, and P. Wadhams, Field experiments on Antarctic tabular icebergs, *Polar Rec., 20*(128), 445–448, 1981.

Kristensen, M., V. A. Squire, and S. C. Moore, Tabular icebergs in ocean waves, *Nature, 297*, 669–671, 1982.

Larsen, L. H., Surface waves and low frequency noise in the deep ocean, *Geophys. Res. Lett., 5*(6), 499–501, 1978*a*.

Larsen, L. H., The effects of finite depth on the propagation of non linear wave packets, *J. Phys. Oceanogr., 8*(5), 923–925, 1978*b*.

Larsen, L. H., An instability of packets of short gravity waves in waters of finite depth, *J. Phys. Oceanogr., 9*(6), 1139–1143, 1979

Manley, T. O., L. A. Codispoti, K. L. Hunkins, H. R. Jackson, E. P. Jones, V. Lee, S. Moore, J. Morison, T. T. Packard, and P. Wadhams, The *Fram-3* Expedition, *Eos Trans. AGU, 63*(35), 627–636, 1982.

Mognard, N. M., W. J. Campbell, R. E. Cheney, J. G. Marsh and D. B. Ross, Southern ocean waves and winds derived from SEASAT altimeter measurements, in *Wave Dynamics and Radio Probing of the Ocean Surface*, Plenum, New York, in press, 1983.

Moore, S. C., and P. Wadhams, Recent developments in strainmeter design, in *Proceedings of Workshop on Sea Ice Field Measurement*, edited by A. J. Allan and D. P. Bazeley, pp. 97–125, Memorial University, St. John's, Newfoundland, 1980.

Munk, W. H., G. R. Miller, F. E. Snodgrass, and N. F. Barber, Directional recording of swell from distant storms, *Philos. Trans. R. Soc. London, Ser. A, 255*, 505–584, 1963.

Orheim, O., Physical characteristics and life expectancy of tabular Antarctic icebergs, *Ann. Glaciol., 1*, 11–18, 1980.

Orheim, O., P. Wadhams, and M. Kristensen, Iceberg response to sea state, *Iceberg Res., 1*, 10–15, 1982.

Robin, G. de Q., S. Evans and J. T. Bailey, Interpretation of radio echo sounding in polar ice sheets, *Philos. Trans. R. Soc. London, Ser. A, 265*(1166), 436–505, 1969.

Smith, S. D., and E. G. Banke, A numerical model of iceberg drift, paper presented at the 6th International Conference on Port and Ocean Engineering, Under Arctic Conditions, Univ. Laval, Quebec, July 1981.

Sodhi, D. S., and M. El-Tahan, Prediction of an iceberg drift trajectory during a storm, *Ann. Glaciol., 1*, 77–82, 1980.

Squire, V. A., An investigation into the use of strain rosettes for the measurement of propagating cyclic strains, *J. Glaciol., 20*(83), 425–431, 1978.

Squire, V. A., Numerical simulation of ice floes in waves, *Tech. Rep. 81-1*, 57 pp., Scott Polar Res. Inst., Cambridge, 1981.

Vinje, T., Some satellite-tracked iceberg drifts in the Antarctic, *Ann. Glaciol., 1*, 83–87, 1980.

Wadhams, P., The seasonal ice zone, in *The Geophysics of Sea Ice, Proceedings of the NATO Advanced Study Institute on Air-Sea Interaction in the Presence of Ice*, edited by N. Untersteiner, Plenum, in press, 1983.

Weeks, W. F., and M. Mellor, Some elements of iceberg technology, *Iceberg Utilization*, edited by A. A. Husseiny, pp. 45–98, Pergamon, New York, 1978.

(Received December 23, 1982;
revised April, 18, 1983;
accepted April 8, 1983.)